

Enhancement of laser wakefield acceleration generated electron beam energies on Gemini by employing $f/40$ focussing

Contact: k.poder12@imperial.ac.uk

K. Poder, J. C. Wood, N. Lopes, S. Alatabi, J. M. Cole, C. Kamperidis, A. Sahai, S. P. D. Mangles and Z. Najmudin
The John Adams Institute for Accelerator Science, Imperial College, London, SW7 2BZ, United Kingdom

P. S. Foster, D. Rusby, D. R. Symes
Central Laser Facility, Rutherford Appleton Laboratory, Didcot, OX11 0QX, United Kingdom

O. Kononenko, C. A. J. Palmer
Deutsches Elektronen-Synchrotron DESY, D-22607 Hamburg, Germany

J. R. Warwick, G. Sarri
Queen's University Belfast, Belfast, BT7 1NN, United Kingdom

Abstract

Experimental electron acceleration results from the 250 TW Gemini laser are presented. The maximum electron beam energy generated from a single stage laser wakefield accelerator was increased beyond 2 GeV by using a focussing optic with an increased focal length. The peak electron beam energy was measured to be more than doubled when employing $f/40$ focussing compared to results obtained with $f/20$. Three-dimensional particle-in-cell simulations reveal that the smoother transverse self-focussing and pulse compression arising from longer focussing optic result in much less wake evolution, allowing the self-injected electrons to accelerate in regions with highest electric fields for much longer.

Introduction

The last few years have seen the peak electron beam energy from laser wakefield accelerators (LWFAs) extended from tens of MeVs [1–3] to the multi-GeV regime by using petawatt lasers [4], implementing staging [5] or by employing external guiding structures [6]. In fact, many examples of the highest energies from LWFAs have been achieved by employing plasma waveguides. The use of such preformed plasma channels [7] allows for greater interaction distances, however, it also increases the sensitivity to input pointing fluctuations which can lead to damage from mis-aligned high power shots. Thus, while being advantageous, plasma waveguides present their own challenges.

In the self-guided regime [8], the maximum single stage energy gain has been pushed to 2 GeV by increasing the laser power to 1 PW [4]. However, it would be preferable to reach higher energy gains without such dramatic increase in laser power, or the extra experimental complications that arise from external guiding structures.

The maximum single stage electron energy scales in the 3D non-linear regime as $\Delta W = 2a_0 n_c / (3n_e) m_e c^2$,

where $a_0 = eE_0 / (m_e c \omega_0)$ is the normalised vector potential of the laser with peak electric field E_0 and $n_c = m_e \epsilon_0 \omega_0^2 / e^2$ is the critical density [9]. In this regime the matched laser spot size w_m scales as $k_p w_m = 2\sqrt{a_0}$, where $k_p = \omega_p / c$ is the plasma wavenumber. Thus the guided laser mode size scales as $w_m \propto 1/n_e^2$ on plasma density and $w_m \propto 1/I_L^4$ in laser intensity. Combining these two expressions allows one to express the single stage energy gain of self-guided LWFAs as

$$\Delta W = \frac{1}{6} \frac{\omega_0^2}{c^2} w_m^2 m_e c^2. \quad (1)$$

The above scaling is valid as long as the laser power is above the critical power for self-focussing and $a_0 \gtrsim 2$. Thus, for LWFA driven by a laser with a spot size that is matched to the plasma density, the total energy gain scales as the square of the spot size in the 3D non-linear regime. This means that increasing the vacuum spot size and correspondingly changing plasma conditions to match the laser spot size and intensity allows for the increase of electron energy gains for a fixed power laser. Hence we investigated doubling the laser spot size by using a longer focal length optic to potentially drive LWFA at a lower density, thus increasing the electron beam energy.

Experimental set up

The experiments were carried out using the Gemini laser. Linearly polarised laser pulses with a central wavelength of 800 nm, gaussian temporal profile with a FWHM duration of $\tau = 45$ fs and energy up to 9.5 J were focussed with a $f = 6$ m spherical mirror (F-number of 40) to an elliptical spot with the e^{-2} intensity minor and major semi-axes of $w_{\text{minor}} = (37 \pm 2) \mu\text{m}$ and $w_{\text{major}} = (48 \pm 2) \mu\text{m}$. The average energy within the $1/e$ contour of intensity was $(50 \pm 5) \%$. The peak vacuum intensity with $E_L = 10$ J was calculated to be $I_{\text{peak}} = (6.2 \pm 0.8) \times 10^{18} \text{ W cm}^{-2}$, corresponding to a

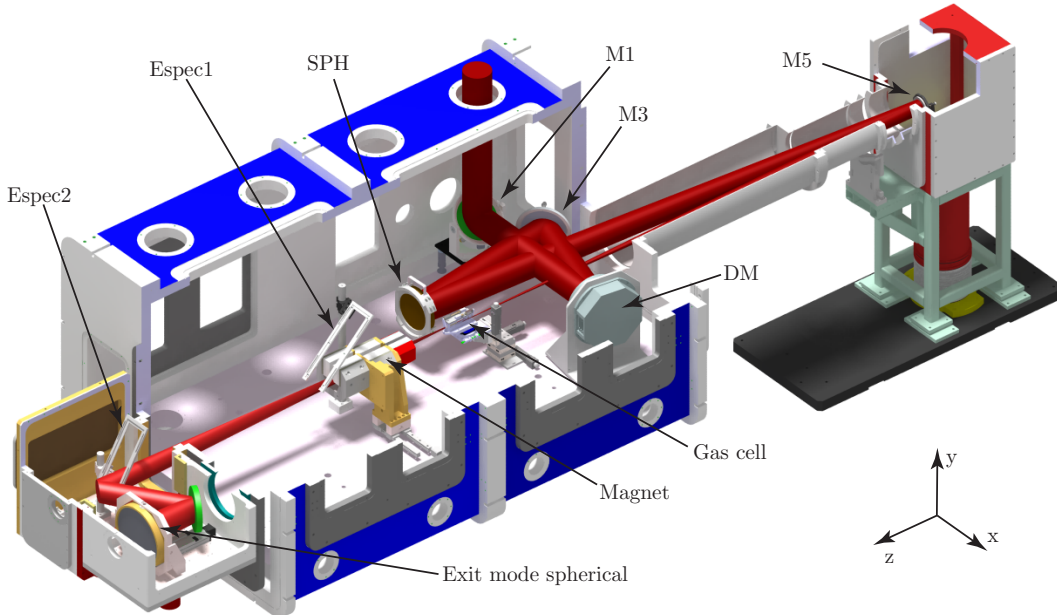


Figure 1: CAD cutaway drawing showing the principal experimental setup.

normalised peak vector potential of $a_0 = 1.7 \pm 0.1$. For reduced laser energies E_{laser} , the peak vector potential scales as $a_0 = 1.7 \cdot (E_{\text{laser}}/10)^{1/2}$.

The principal experimental setup is shown in Figure 1. The laser is reflected off a deformable mirror DM at the shallowest angle possible as the focussing optic used is a spherical mirror. The deformable mirror is used to optimise the spatial phase of the pulse and to correct for astigmatism arising from using the spherical mirror SPH off-axis. The beam is then folded using a high damage threshold dielectric-coated mirror, M5 in Figure 1. The fluence on this optic is about 4 times higher than in the laser nearfield and damage was observed to occur with highest laser energies. The transmission through the folding mirror was measured by imaging a scattering screen placed behind it; this was a diagnostic to allow the reflectivity of the mirror to be monitored. A large increase in signal behind the mirror indicated failure of the optic.

The target used in this campaign was a custom designed, variable length gas cell. Its length can be continuously changed between 3 mm and 42 mm. The plasma density in the gas cell was measured on every shot by using moiré interferometry. A trace of the pressure in the gas cell was saved on every shot. In order to improve shot-to-shot fluctuations, a newly built gas delivery system was employed, reducing variations in pressure by a factor of ten.

The magnetic spectrometer used to characterise electron beams consisted of a 42 cm long, $\langle B \rangle = 0.95$ T dipole magnet and two spectrometer screens. Errors arising from poor imaging or misread positions on screen can be evaluated by calculating the difference between actual and measured energy. Such errors arising for a

measurement offset of 1 mm are always below 1% for Screen 2 for energies up to 3 GeV.

Experimental results

Plasma density was scanned under the optimum laser parameters, delivering a peak energy of 11 J on target. This was the highest intensity achieved during the experimental campaign, corresponding to a peak normalised vector potential of $a_0 = 1.8$ and a laser power of $P_L \simeq 240$ TW. Plasma density was varied in the range of $1.6 \times 10^{18} \text{ cm}^{-3} < n_e < 3.3 \times 10^{18} \text{ cm}^{-3}$ while the gas cell length was kept fixed at $L_{\text{cell}} = 20$ mm. Raw electron spectrometer data taken at different plasma densities is shown in Figure 2. The electron beam energy increases horizontally; the vertical dimension is proportional to beam divergence. An increase in maximum energy is evident with rising plasma density, up to a maximum at $n_e = 2.8 \times 10^{18} \text{ cm}^{-3}$ where electron energies well in excess of 2 GeV are measured. After that the electron beam energy stops increasing and instead a beam at lower energies with much larger divergence is observed. A greater amount of charge is observed with increased plasma density as well, increasing from a few pC at $n_e = 1.8 \times 10^{18} \text{ cm}^{-3}$ to $Q_{\text{tot}} \gtrsim 300$ pC at the highest densities of $n_e \simeq 3 \times 10^{18} \text{ cm}^{-3}$. Interestingly, at the lowest plasma densities a low charge quasi-monoenergetic electron beam is observed; the FWHM energy spread measured with $n_e = 1.8 \times 10^{18} \text{ cm}^{-3}$ is 9%.

The variation of peak energy with plasma density witnessed in Figure 2 is counter-intuitive. Instead of the expected n_e^{-1} scaling the cut-off energy raises with increasing plasma density. The maximum electron energy

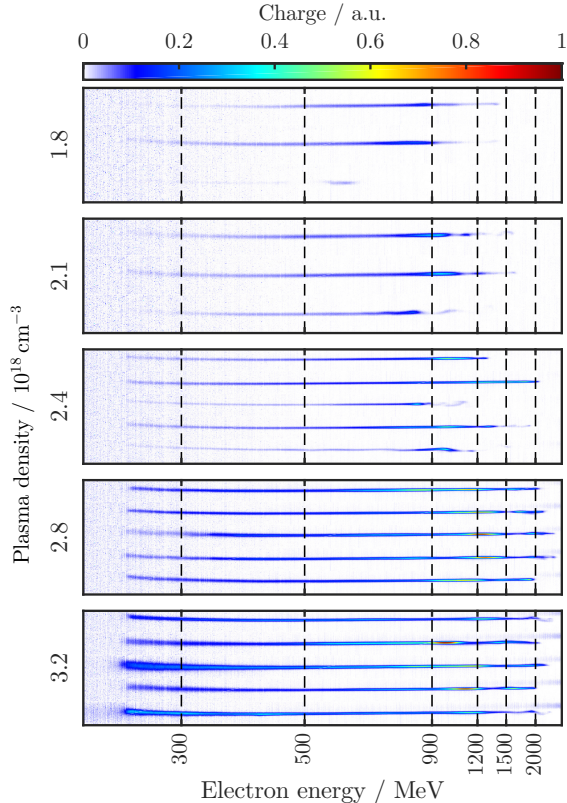


Figure 2: Raw electron spectrometer data from a plasma density scan with gas cell length of 20 mm.

peaks at $n_e \simeq 3 \times 10^{18} \text{ cm}^{-3}$ and rolls over for higher densities. The initial rise of electron energy with plasma density is caused by two effects. Firstly, injection will be occurring earlier in the interaction as the plasma density increases, due to faster self-focussing and compression of the pulse. Secondly, at lower plasma densities the accelerating field will be smaller. The reason for this is twofold: a_0 will be smaller at a lower plasma density supporting a larger matched spot size and the electric field scales as $E_z \propto \sqrt{a_0 n_e}$. Thus, the total energy gain is limited as the target length is fixed.

Spectra for single shots taken at the conditions yielding the highest energy electron beams are plotted in Figure 3. All these shots have been propagated backwards through the magnetic spectrometer to correct for pointing variations of the electron beam. A large shot-to-shot variability is evident, however, the beams always reach multi-GeV energies. For shot 5 plotted in Figure 3, the total beam charge in electrons with $\mathcal{E} > 200 \text{ MeV}$ is measured to be $Q_{\text{tot}} \simeq 370 \text{ pC}$, corresponding to a total beam energy of at least 0.34 J . The total charge of electrons with energies beyond 2 GeV was measured as $Q_{\mathcal{E} > 2 \text{ GeV}} = 15 \text{ pC}$; this corresponds to 33 mJ of beam energy. Thus, up to 10% of the total beam energy is concentrated in electrons with $\mathcal{E} > 2 \text{ GeV}$; more than half the beam energy for Shot 5 in Figure 3 is carried by electron with energies beyond 1 GeV . Thus these results represent a truly multi-gigaelectronvolt laser wake-

field accelerator. Also, these beam energies represent the highest reported electron energies in the self-guided, self-injection regime of laser wakefield accelerators for laser power below 1 PW . Finally, the conversion efficiency from laser energy to electron beam energy can be estimated to be $\eta = 0.34 \text{ J}/11 \text{ J} \simeq 3\%$; note this is the lower boundary on the value as the amount of charge in electrons with energies below 200 MeV is not measured.

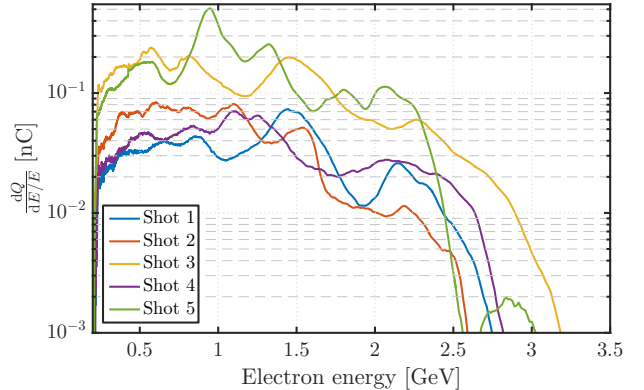


Figure 3: Single shot electron spectra for the highest electron energies obtained, measured with $n_e = 2.8 \times 10^{18} \text{ cm}^{-3}$ and gas cell length of 20 mm.

Simulations

In order to understand the intricacies of the acceleration process three-dimensional particle-in-cell simulations were carried out employing the EPOCH code[10]. As the spatial wavefront was not measured the simulations could only be performed to understand the qualitative differences between the different focussing geometries [11]. To simulate the $f/40$ interaction, a linearly polarised laser pulse with $\tau_{\text{FWHM}} = 45 \text{ fs}$ and a transverse elliptical gaussian profile with $w_y = 48 \mu\text{m}$ and $w_z = 36 \mu\text{m}$ and a peak normalised vector potential of $a_0 = 2$ was focussed 0.5 mm into the plasma. The plasma profile consisted of a 0.5 mm linear ramp followed by a plateau of $n_e = 3 \times 10^{18} \text{ cm}^{-3}$. The simulation box size was $80 \times 280 \times 220 \mu\text{m}^3$ and propagates along the x -axis with the group velocity of the laser. A total of 1.2×10^9 particles were used; the grid resolution was set to $k_0 \Delta x = 0.21$ and $k_p \Delta y = k_p \Delta z = 0.13$. Additional simulations were performed with a laser spot and box size half of that described above to gain understanding of the quantitative differences between electron acceleration dynamics between the $f/40$ and $f/20$ focussing.

Figure 4 presents the results of the 3D simulations. Panels (a) and (b) show the electron beam energy spectrum as a function of propagation distance x for the $f/40$ and $f/20$ simulations, respectively. As was witnessed in the experiment, the longer focal length simulation produces electron beams with higher peak energies. The maximum beam energy is $\mathcal{E}_{f/40} \simeq 1.8 \text{ GeV}$ for the $f/40$ simulation while the highest energies reached in the $f/20$

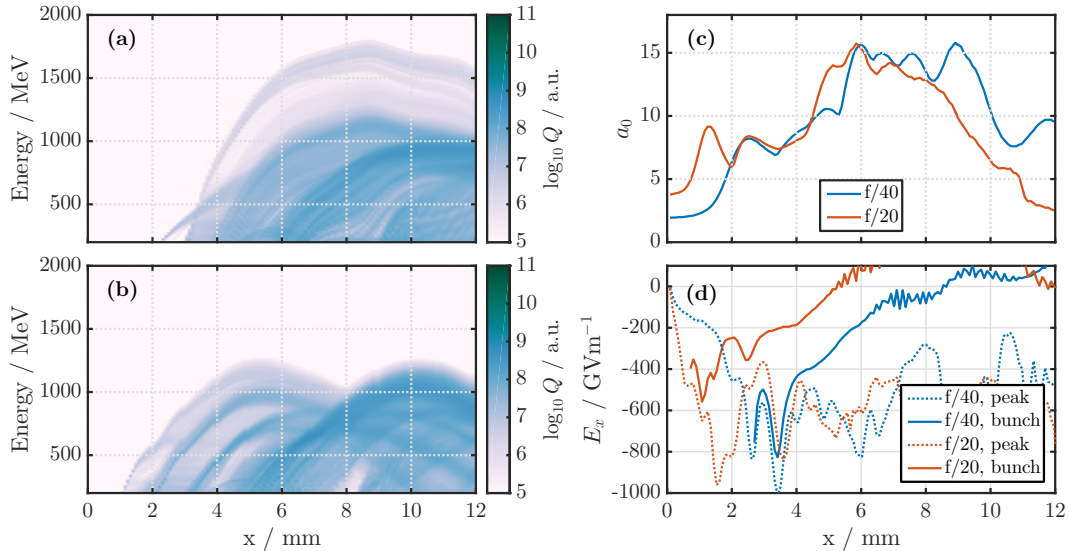


Figure 4: Simulation results highlighting the different laser and electron beam dynamics, showing enhanced electron acceleration with extended focussing.

simulation were $\mathcal{E}_{f/20} \simeq 1.3$ GeV.

Panel (c) in Figure 4 depicts the evolution of a_0 throughout the simulations. In the case of the $f/20$, there is rapid self-focussing at the beginning of the interaction and the laser intensity is amplified to more than twice its vacuum value after $x \simeq 1.5$ mm. This leads to self-injection of electrons very early in the interaction, as seen in Figure 4b. However, due to ongoing pulse evolution the electron bunch is frequently rephased within the bubble. This is shown in Figure 4d plotting the average longitudinal electric field within the bubble as a function of propagation experienced by the electron population highlighted in Panels (a) and (b). Also plotted in Figure 4d as the dotted line is the peak accelerating gradient within the bubble as a function of propagation. The electron bunch in the $f/20$ simulation is injected very close to the peak gradient but rapid pulse evolution rephases the bunch within the bubble such that the accelerating field felt by the bunch is reduced greatly. Overall this limits the energy gain of the electrons.

Different behaviour is observed for the $f/40$ case. The laser intensity amplification is smoother and slower, as observed in Figure 4c, leading to self-injection at $x \simeq 3$ mm. As seen from Figure 4d, the bunch is again injected very close the peak gradient. Contrasting with the $f/20$ case, however, the injected electron bunch stays in a phase with very high accelerating field. This is caused by the smoothness of laser intensity evolution, leading to the bubble being quasi-static. Thus the high initial intensity of the $f/20$ causes large and frequent variations in the laser intensity, leading to a highly volatile bubble which in turn leads to electron rephasing into phases with lower electric fields. This is avoided with the longer focal length and lower initial intensity, enabling extended electron energy gains.

Conclusion

The maximum electron beam energy obtained from a self-guided, self-injecting laser wakefield accelerator driven by the Gemini laser was extended beyond 2 GeV by using a longer focal length focussing geometry. Up to 10% of the total electron beam energy was measured to be carried by electrons with energies in excess of 2 GeV at optimum plasma conditions. Compared to the standard $f/20$ focussing, employing the $f/40$ setup more than doubled the electron energies. Particle-in-cell simulations comparing $f/20$ and $f/40$ focussing reveal much more stable self-focussing dynamics for the extended focal length. The large fluctuations in laser intensity in the $f/20$ case result in electron bunch rephasing within the wake, resulting in limited energy gains. Contrastingly, the $f/40$ focussing results in smoother bubble evolution and injection into a stable wake, allowing for enhanced electron acceleration.

Acknowledgements

The authors would like to thank Gemini target area staff and laser operators along with CLF engineering. We acknowledge funding from STFC for the support of the John Adams Institute of Accelerator Science by grants ST/J002062/1 and ST/P000835/1. The simulations were performed using Imperial College High Performance Computing Service. The EPOCH code used in this research was developed under UK Engineering and Physics Sciences Research Council grants EP/G054940/1, EP/G055165/1 and EP/G056803/1

References

1. Mangles, S. P. D. *et al.* Monoenergetic beams of relativistic electrons from intense laserplasma interactions. *Nature* **431**, 535–538 (2004).
2. Faure, J. *et al.* A laserplasma accelerator producing monoenergetic electron beams. *Nature* **431**, 541–544 (2004).
3. Geddes, C. G. R. *et al.* High-quality electron beams from a laser wakefield accelerator using plasma-channel guiding. *Nature* **431**, 538–541 (2004).
4. Wang, X. *et al.* Quasi-monoenergetic laser-plasma acceleration of electrons to 2 GeV. *Nature Communications* **4**. doi:10.1038/ncomms2988 (2013).
5. Kim, H. T. *et al.* Enhancement of Electron Energy to the Multi-GeV Regime by a Dual-Stage Laser-Wakefield Accelerator Pumped by Petawatt Laser Pulses. *Physical Review Letters* **111**, 165002 (2013).
6. Leemans, W. P. *et al.* Multi-GeV Electron Beams from Capillary-Discharge-Guided Subpetawatt Laser Pulses in the Self-Trapping Regime. *Physical Review Letters* **113**, 245002 (2014).
7. Butler, A., Spence, D. J. & Hooker, S. M. Guiding of High-Intensity Laser Pulses with a Hydrogen-Filled Capillary Discharge Waveguide. *Physical Review Letters* **89**, 185003 (2002).
8. Kneip, S. *et al.* Near-GeV Acceleration of Electrons by a Nonlinear Plasma Wave Driven by a Self-Guided Laser Pulse. *Physical Review Letters* **103**, 035002 (2009).
9. Lu, W., Huang, C., Zhou, M., Mori, W. B. & Katsouleas, T. Nonlinear Theory for Relativistic Plasma Wakefields in the Blowout Regime. *Physical Review Letters* **96**, 165002 (2006).
10. Arber, T. D., Bennett, K., Brady, C. S. & Ramsay, M. G. Contemporary particle-in-cell approach to laser-plasma modelling. *Plasma Physics and Controlled Fusion* **57**, 113001 (2015).
11. Ferri, J. *et al.* Effect of experimental laser imperfections on laser wakefield acceleration and betatron source. *Scientific Reports* **6**, 27846 (2016).